Journal of Statistical Physics, Vol. 83, Nos. 3/4, 1996

Numerical and Analytical Studies of Nonequilibrium Fluctuation-Induced Transport Processes

T. C. Elston[1] and Charles R. Doering[1]

Received March 14, 1995; final July 5, 1995

We present a numerical simulation algorithm that is well suited for the study of noise-induced transport processes. The algorithm has two advantages over standard techniques: (1) it preserves the property of detailed balance for systems in equilibrium and (2) it provides an efficient method for calculating nonequilibrium currents. Numerical results are compared with exact solutions from two different types of correlation ratchets, and are used to verify the results of perturbation calculations done on a three-state ratchet.

KEY WORDS: Algorithm; stochastic; transport; ratchets; nonequilibrium; detailed balance; master equation; jump process.

1. INTRODUCTION

Noise-induced transport processes recently have received considerable attention.[1-12] The focus of these studies has ranged from intracellular transport processes[1,4,5] to novel mass separation techniques based on thermal diffusion.[10] Thermal fluctuations are a dominant factor in all biological processes that occur at the subcellular level, and it is conceivable that nature has evolved mechanisms to take advantage of this noisy environment. New experimental techniques have made it possible to study the motion of single motor molecules such as kinesin.[13,14] These experiments have led to considerable insight into the mechanisms used by motor molecules to perform directed motion. As more experimental data have become available, the theoretical models used to describe these processes have become increasingly complex.[15] Hence it is important that efficient and reliable numerical methods are available for studying these processes.

[1] Center for Nonlinear Studies, MS-B258, Los Alamos National Laboratory, Los Alamos, New Mexico 87545; E-mail: elston@cnls.lanl.gov, doering@cnls.lanl.gov.

0022-4715/96/0500-0359$09.50/0

When studying noise-induced transport, the property of interest is the steady-state current produced by the system. The existence of a net drift indicates the ability of the system to perform useful work. Often the currents produced by these systems are quite small as compared to the magnitude of the noise. It is therefore important that numerical algorithms used to simulate these systems do not produce a net drift as a result of numerical error. A minimum requirement for a reliable algorithm is that it preserves the property of detailed balance for equilibrium processes. One is then more confident that the currents produced when the system is driven away from equilibrium are a direct result of the applied external forces and are not numerical artifacts. The relatively large fluctuations inherent in these systems also make the standard procedure of calculating currents by averaging over many realizations of the stochastic process extremely time-consuming.

With these considerations in mind, we present a novel algorithm for numerically simulating a class of stochastic processes. While elements of this numerical scheme have previously been used in chemical kinetics and Monte Carlo simulations, we believe that our application of these ideas represents a new technique for studying noise-induced transport and other stochastic processes. In Section 2 we present the details of how the algorithm works. In Section 3 we introduce the correlation ratchet as a generic model for noise-induced transport processes. The numerical results of our algorithm are then compared against exact results for two types of correlation ratchets. Finally, in Section 4 we present asymptotic perturbation calculations done on a three-state model of a correlation ratchet. The validity of these expressions is then verified using our algorithm. Because the perturbation technique is itself a powerful tool for studying noise-induced transport processes, the details of the calculations are sketched in the appendix.

2. THE ALGORITHM

To motivate our numerical scheme, we first consider a simple system that consists of an overdamped particle subjected to thermal noise and a force due to the potential $v(x)$. Initially we assume that the form of the potential $v(x)$ leads only to bounded motion. The Fokker–Planck equation for the conditional probability density ρ for this process is

$$\frac{\partial \rho}{\partial t} = \frac{\partial v'(x)\,\rho}{\partial x} + KT\frac{\partial^2 \rho}{\partial x^2} \tag{1}$$

where K is the Boltzmann constant, T is the absolute temperature, and the time t has been scaled by the reciprocal of the friction coefficient. Equation (1) may be written in the equivalent form

$$\frac{\partial \rho}{\partial t} + \frac{\partial J}{\partial x} = 0 \tag{2}$$

where $J = -v'(x)\,\rho - KT\partial_x \rho$ is the probability current. Equation (2) has the form of an equation of continuity and expresses the fact that probability is neither created nor destroyed. The stationary probability density ρ_S of this process is found by setting the left-hand side of Eq. (1) equal to zero. Doing this gives

$$\rho_s = \frac{e^{-v(x)/KT}}{Z} \tag{3}$$

where Z is the appropriate normalization constant. Equation (3) is consistent with the probability distribution found from equilibrium statistical mechanics. For this process the equilibrium probability current vanishes, which implies detailed balance.[16]

Single realizations of the stochastic process described by (1) are produced from the Langevin equation

$$\frac{dx}{dt} = -v'(x) + (2KT)^{1/2}\,\tilde{g} \tag{4}$$

where $\tilde{g}$ is a Gaussian white noise term whose mean and variance are given by

$$\langle g(t) \rangle = 0 \tag{5}$$

$$\langle g(t)\, g(s) \rangle = \delta(t-s) \tag{6}$$

The simplest approach for numerically simulating Eq. (4) is by discretizing time and using an Euler-type algorithm for advancing $x(t_n)$ to $x(t_{n+1})$. This is done as follows:

$$x(t_{n+1}) = x(t_n) - \Delta t\, v'(x_n) + (2KT\,\Delta t)^{1/2}\,\psi_n \tag{7}$$

where Δt is the time step and ψ_n is a Gaussian-distributed random variable with zero average and a variance of unity, independently chosen at each time step.

Instead of discretizing time, we could just as easily discretize the dependent variable x. Making x discrete converts the problem into a jump

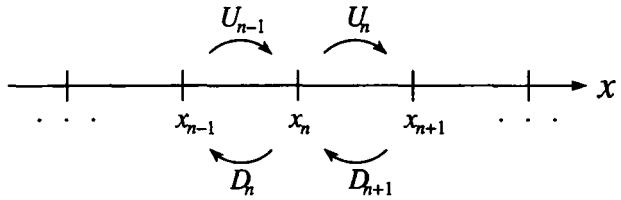

Fig. 1. The jump process used to approximate the stochastic process.

process.[2] That is, we must now consider the rates at which jumps occur out of x_n and into either x_{n-1} or x_{n+1} and the corresponding reverse transitions. This situation is depicted in Fig. 1. The master equation for this process is

$$\frac{dP_n}{dt} = U^{n-1}P^{n-1} - D^nP^n + D^{n+1}P^{n+1} - U^nP^n \tag{8}$$

where P_n is the probability for being at site x_n at time t, U^n is the rate at which transitions occur from x_n to x_{n+1} and D^n is the rate at which transitions occur from x_n to x_{n-1}. We are now left with the problem of determining the appropriate values of U^n and D^n to use for this process. To find these values, we first consider the stationary probability density given by Eq. (2). One criterion for Eq. (8) to be a valid approximation to the stochastic process we are considering is that the stationary probability P_n^S for being at site x_n is

$$P_n^s = \frac{\Delta x\, e^{-v(x_n)/KT}}{Z} \tag{9}$$

Since Eq. (8) is being used to describe an equilibrium process, the condition of detailed balance must be enforced. This requirement can be expressed as

$$D^{n+1}P^{n+1} = U^nP^n \tag{10}$$

Together Eqs. (9) and (10) imply

$$\frac{P^{n+1}}{P^n} = \frac{U^n}{D^{n+1}} = e^{-[v(x_{n+1}) - v(x_n)]/KT} \tag{11}$$

[2] A numerical scheme similar to the one proposed here has also been developed by Peskin (see ref. 15).

A choice for the rates U^n and D_n that is consistent with (11) is

$$U^n = \frac{KT}{\Delta x^2} e^{-[v(x_{n+1}) - v(x_n)]/2KT} \tag{12}$$

$$D^n = \frac{KT}{\Delta x^2} e^{[v(x_n) - v(x_{n-1})]/2KT} \tag{13}$$

The prefactors in front of the exponentials in Eqs. (12) and (13) have been chosen so that if terms of $o(\Delta x^2)$ are neglected, then (8) is equivalent to a second-order finite differencing of Eq. (1).[17]

Equation (8) can now be used to generate directly realizations of the stochastic process under consideration. This is done in the following way. We start the particle at an initial site x_n. The amount of time the particle waits at this site is an exponentially distributed random variable characterized by its mean value

$$\langle t \rangle = \frac{1}{D^n + U^n} \tag{14}$$

The computer generation of exponentially distributed random numbers is accomplished by using the formula

$$t = \frac{-1}{D^n + U^n} \ln(X) \tag{15}$$

where X is a uniformly distributed random number between zero and one. To determine which way the particle moves, a second uniformly distributed random number is generated by the computer. This number is then compared against the probability of a jump from x_n to x_{n+1},

$$P(x_n \to x_{n+1}) = \frac{U^n}{D^n + U^n} \tag{16}$$

and the probability of a jump from x_n to x_{n-1},

$$P(x_n \to x_{n-1}) = \frac{D^n}{D^n + U^n} \tag{17}$$

By repeating this procedure, we generate individual realizations of the stochastic process described by (8). Note that no approximations have been used in generating these realizations. The approximation in this scheme is in going from the Fokker–Planck equation (1) to the master equation (8). As the master equation (11) possesses detailed balance, we are guaranteed that our scheme respects this property.

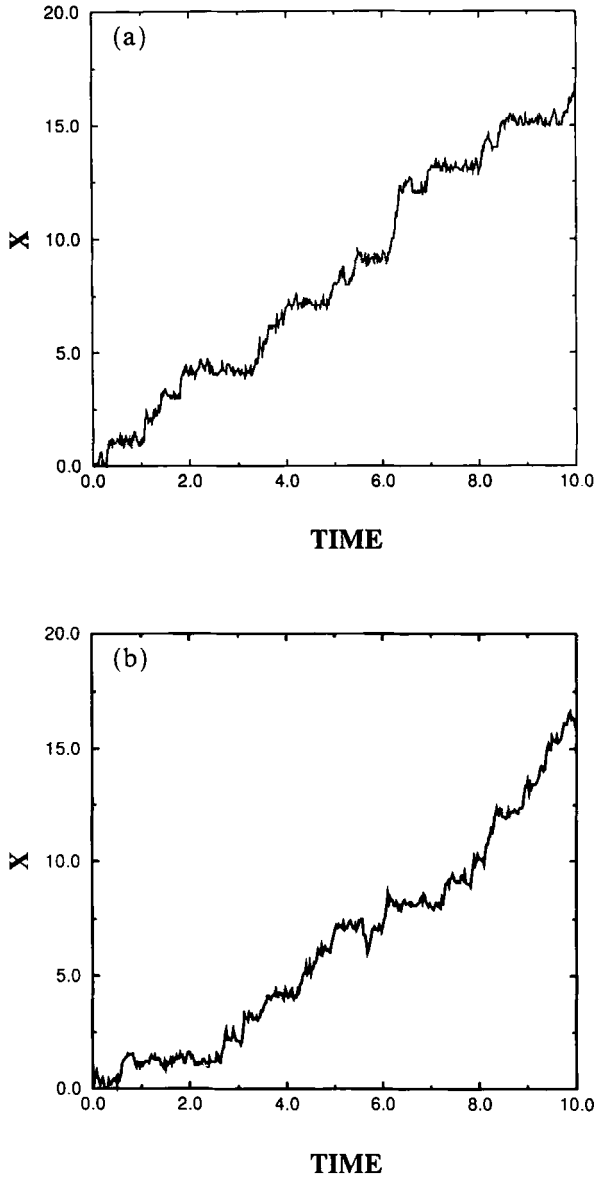

Fig. 2. (a) A realization of the stochastic process described by Eq. (18) using the discrete-space method. The parameters used to generate this figure were $E = 10.0$, $\alpha = 10/11$, $F = 1.0$, $KT = 1.0$, and $\Delta x = 0.05$. (b) A realization of the same stochastic process as shown in (a). For this case time was taken to be discrete. The time step used in this figure was $\Delta t = 0.0025$. (c) A piecewise linear potential. The maximum height of the potential is E and occurs at $x = \alpha$.

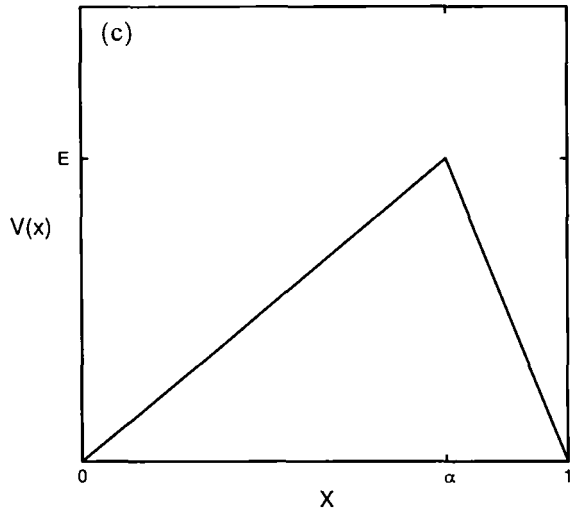

Fig. 2. (*Continued*)

This algorithm is easily generalizable to include all gradient systems. As an example consider the following nonequilibrium system:

$$\frac{dx}{dt} = -v'(x) + F + \tilde{g} \tag{18}$$

For this process the potential to be used in determining the transitions rates is

$$U(x) = v(x) - Fx \tag{19}$$

which gives the following expressions for U^n and D^n:

$$U^n = \frac{KT}{\Delta x^2} e^{-[v(x_{n+1}) - v(x_n) - F\Delta x]/2KT} \tag{20}$$

$$D^n = \frac{KT}{\Delta x^2} e^{[v(x_n) - v(x_{n-1}) - F\Delta x]/2KT} \tag{21}$$

$$\tag{22}$$

In Fig. 2a we show a realization of Eq. (18) using our algorithm. The potential $v(x)$ used to generate Fig. 2a was the periodic piecewise linear potential shown in Fig. 2c. The maxium height E of the potential was taken to be 5 and the position α where this maximum occurs was 5/6. The

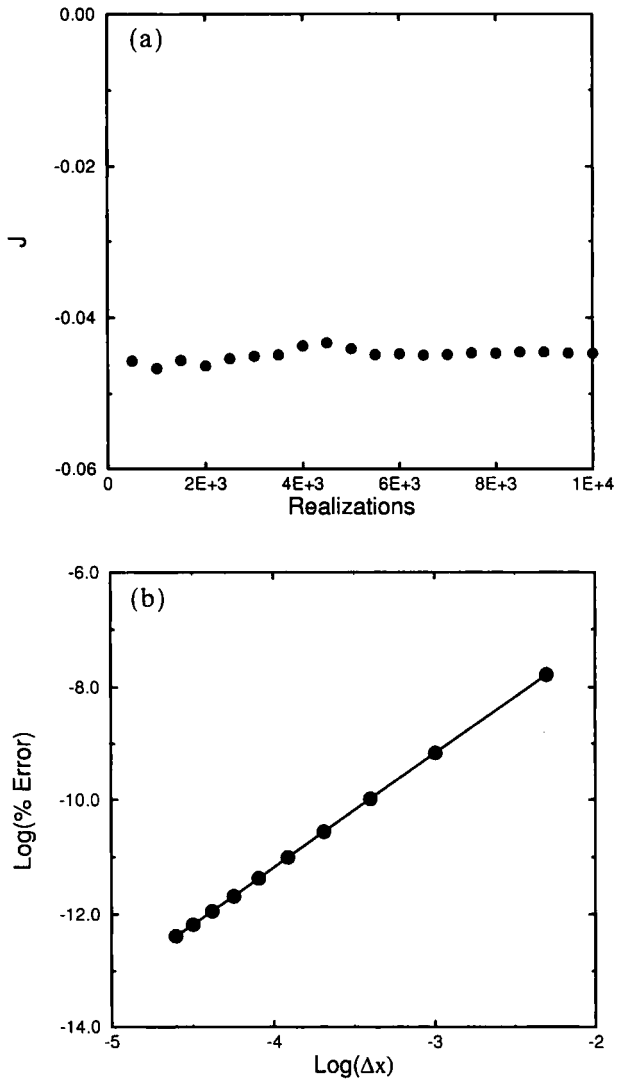

Fig. 3. (a) A plot of the current versus number of realizations. The parameters used to generate this figure were the same as in Fig. 2b, except $F = 0$. The measured current is a result of numerical error. (b) A plot of the log of the percent error in the numerically calculated current versus the log of the step size.

strength of the added force F was 4.0, $\Delta x = 0.05$, and $KT = 1$. In Fig. 2b a realization of the same process using the standard Euler method is shown. For comparison, the time step was chosen according to conventional diffusive scaling, $\Delta t = \Delta x^2/KT = 0.0025$. Figures 2a and 2b are not identical, as they correspond to two distinct realizations of a random process. From visual inspection, the size of the fluctuations and the average drift appear to be identical in the two plots, but qualitative differences are apparent.

If the driving force F is set equal to zero and $v(x)$ is taken to be periodic, then the system described by (18) should produce no net drift. Figure 3a shows a plot of the net current versus the number of realizations used to calculate the current. The same potential and parameter values as in Fig. 2b were used to generate this figure. The current is clearly converging to a nonzero value, illustrating the effects of numerical error. As a simple example to illustrate the second-order accuracy of our algorithm, we use it to calculate the current produced when $v(x)$ is set equal to zero and $F = 1$. For this case the current is simply 1. The method used to calculate the current is described in Section 3. Figure 3b shows a plot of the log of the percent error of the numerically calculated current versus the log of Δx. The slope of the line in Fig. 3b is 2, indicating that the error is decreasing as the square of the step size.

3. RATCHETS

A simple mathematical model of a ratchet is a spatially anisotropic periodic potential. Particles subjected to ratchet potentials plus noise from both thermal and nonequilibrium sources can experience a nonzero average drift. Because these systems are driven by nonequilibrium fluctuations, they have been referred to as correlation ratchets. For a general review of correlation ratchets and the mechanisms that lead to fluctuation-induced currents, the reader is referred to ref. 18. In this section we use two models of correlation ratchets, whose currents can be solved for exactly,[5] to test the accuracy and efficiency of our algorithm.

The general form of the stochastic differential equation describing the two types of ratchets we will consider is

$$\frac{dx}{dt} = -v'(x) - u'(x, t) + (2KT)^{1/2}\,\tilde{g}(t) \tag{23}$$

The time-dependent potential in (23) represents the nonequilibrium fluctuations that drive this process. For simplicity, the fluctuations

in the potential, $u(x, t) \in \{u_+(x), u_-(x)\}$, are governed by the master equation

$$\frac{d}{dt}\begin{pmatrix} P_+(t) \\ P_-(t) \end{pmatrix} = \gamma \begin{pmatrix} -1 & 1 \\ 1 & -1 \end{pmatrix} \begin{pmatrix} P_+ \\ P_- \end{pmatrix} \tag{24}$$

where $P_\pm(t)$ is the probability that $u(x, t) = u_\pm(x)$. Equation (24) represents a dichotomous Markov process in which the potential $u(x, t)$ switches between the two possible values $u_\pm(x)$. The switching between the u_+ and u_- is exponentially correlated and the switching time scale τ_c is determined by the rate γ, i.e., $\tau_c = \gamma^{-1}$. This leads to the following Fokker–Planck equation for the entire process[19]:

$$\frac{\partial}{\partial t}\begin{pmatrix} \rho_+ \\ \rho_- \end{pmatrix} = \begin{pmatrix} L_+(x) - \gamma & \gamma \\ \gamma & L_-(x) - \gamma \end{pmatrix} \begin{pmatrix} \rho_+ \\ \rho_- \end{pmatrix} \tag{25}$$

where

$$L_\pm(x) = \partial_x(v'(x) + u'_\pm(x) + KT\partial_x) \tag{26}$$

Two types of ratchets we will consider are illustrated in Figs. 4a and 4b. In Fig. 4a the fluctuating part of the potential $u(x, t)$ switches between $\mp Fx$. That is, in the first state the particle feels a force due to the periodic potential plus an additional positive constant force F, and in the second state the particle feels the force due to the periodic potential plus an additional negative constant force $-F$. We will call this model the fluctuating-force ratchet to distinguish it from the second model. The second model, illustrated in Fig. 4b, will be termed the fluctuating-potential ratchet. In this case the time-dependent potential $u(x, t)$ fluctuates between the two states $u_\pm(x) = \pm\varepsilon v(x)$.

Using the algorithm described in Section 2, we approximate Eq. (25) by the master equation

$$\frac{dP_{+,n}}{dt} = U_+^{n-1} P_{+,n-1} - D_+^n P_{+,n} + D_+^{n+1} P_{+,n+1} - U_+^n P_{n,+} + \gamma P_{-,n} - \gamma P_{+,n} \tag{27}$$

$$\frac{dP_{-,n}}{dt} = U_-^{n-1} P_{-,n-1} - D_-^n P_{-,n} + D_-^{n+1} P_{-,n+1} - U_-^n P_{-,+} + \gamma P_{+,n} - \gamma P_{-,n} \tag{28}$$

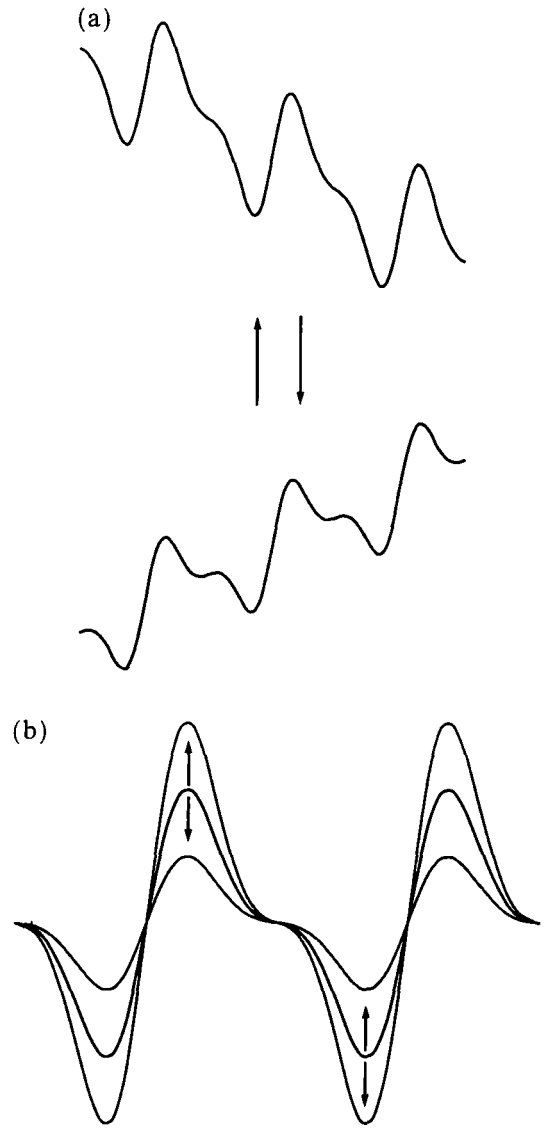

Fig. 4. (a) The fluctuating-force ratchet. (b) The fluctuating-potential ratchet.

where the transition rates are now given by

$$
\begin{aligned}
U_+^n &= \frac{KT}{\Delta x^2} e^{-[v(x_{n+1})+u_+(x_{n+1})-v(x_n)-u_+(x_n)]/2KT} \\
D_+^n &= \frac{KT}{\Delta x^2} e^{[v(x_n)+u_+(x_n)-v(x_{n-1})-u_+(x_{n-1})]/2KT} \\
U_-^n &= \frac{KT}{\Delta x^2} e^{-[v(x_{n+1})+u_-(x_{n+1})-v(x_n)-u_-(x_n)]/2KT} \\
D_-^n &= \frac{KT}{\Delta x^2} e^{[v(x_n)+u_-(x_n)-v(x_{n-1})-u_-(x_{n-1})]/2KT}
\end{aligned}
\tag{29}
$$

In the simplified case that the periodic potential is piecewise linear; the current can be calculated exactly.[5] These models therefore provide a benchmark for testing our algorithm.

The current generated by the jump process that we are using to approximate the correlation ratchets is a function of transition rates U and D and the stationary probabilities $P^s_{\pm,n}$ and is found from the equation

$$
J = U_+^{n-1} P_{+,n-1} - D_+^n P_{+,n} + U_-^{n-1} P_{-,n-1} - D_-^n P_{-,n} \tag{30}
$$

To determine the stationary probabilities, we need only solve the set of coupled linear equations obtained by setting the left-hand side of Eqs. (27) and (28) equal to zero. This procedure should be contrasted with the normal method of averaging over many realizations of Eq. (23) that would have been necessary had we chosen to discretize time. Since Eqs. (27) and (28) are master equations, we are guaranteed that any initial values for the $P_{\pm,n}$ that are consistent with the condition $\sum_n P_{\pm,n} = 1$ will evolve to the same unique stationary distribution.[20] An efficient method of determining the stationary probabilities, therefore, is by numerically integrating Eqs. (27) and (28) forward in time, starting from an appropriate initial condition. The reason this method works well is because the system relaxes exponentially to its stationary state. This method has the added advantage that it eliminates statistical errors associated with averaging over a finite number of realizations. We note that instead of integrating Eqs. (27) and (28) forward in time, we could have solved for the steady-state probabilities directly. This procedure effectively reduces the problem to inverting a $2N$ by $2N$ matrix, where $2N$ is the total number of states in the jump process, and for values of N that are not too large this approach could further reduce computational time.

In Fig. 5 we present the results of our numerical calculations. The solid lines represent the exact analytic values for the current and the diamonds

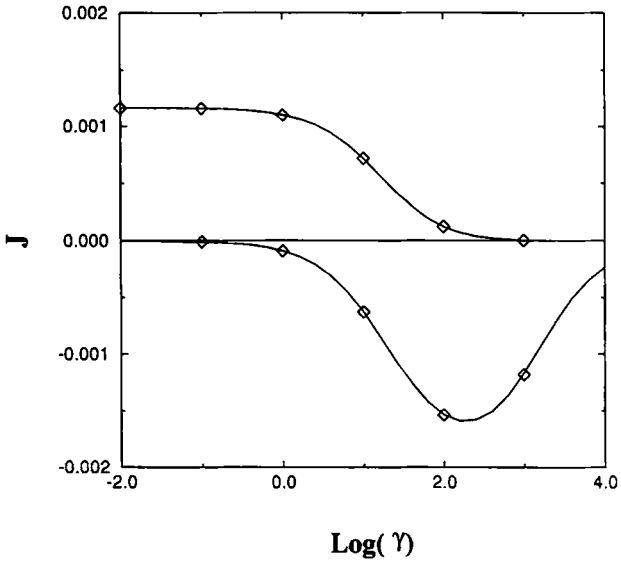

Fig. 5. A plot of the current versus the log of the switching rate. The solid lines are the exact solutions and the diamonds are the results of numerical simulations. The upper curve is for the fluctuating-force ratchet and the lower curve is for the fluctuating-potential ratchet.

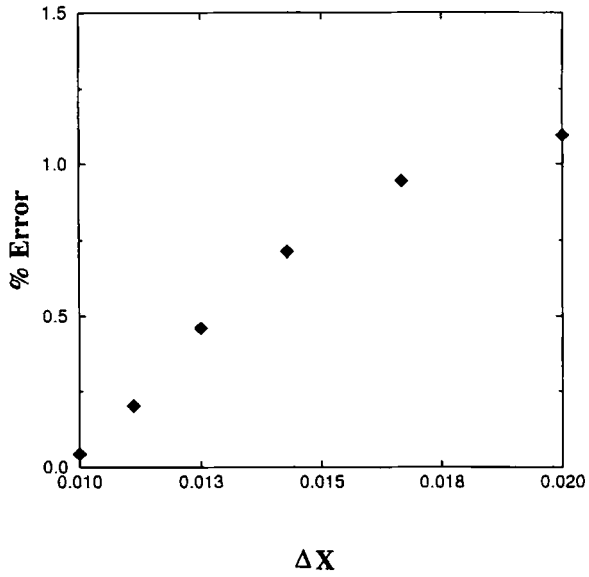

Fig. 6. A plot of the percent error in the numerical value of the current versus step size for the fluctuating-force ratchet. The switching rate γ was 100.

are the values computed numerically. The parameters used to generate this figure were $\alpha = 10/11$, $E = 10$, $\Delta x = 0.01$, and $KT = 1.0$. The upper curve is the current produced by the fluctuating-force ratchet with $F = 1$. The lower curve is the current produced by the fluctuating potential with $\varepsilon = 1$. The figure is a plot of the current versus the log of the switching rate. Note that we get extremely accurate results for over six orders of magnitude of the switching rate. The calculations to produce the data points for both curves took less than 1 hr on a SPARC workstation. Using the discrete-time method and averaging over many realizations of the stochastic process would have required a least 1 day of computing time to get statistics with reasonable error bars.

In Fig. 6 we show a plot of the percent error in the numerical value of the current versus step size for the fluctuating-force ratchet, using the same parameters as in Fig. 5. The switching rate used to generate this plot was $\gamma = 100$. Note that for a step size of 0.02 the error in the current is already close to 1%.

4. A THREE-STATE RATCHET

The dependence of the direction of noise-induced transport on the statistical properties of the nonequilibrium fluctuations was first discussed in ref. 8. In that work the characteristic of the noise that determined the direction of the current was the flatness. The flatness ϕ of a random variable X is defined in terms of its second and forth moments as

$$\phi = \frac{\langle X^4 \rangle}{\langle X^2 \rangle^2} \tag{31}$$

For the two-state ratchets considered in Section 3, the flatness of the nonequilibrium fluctuations is constant, i.e., $\phi = 1$. These systems, therefore, cannot undergo current reversals.

A more robust model is one in which the nonequilibrium fluctuations switch between three different states. Consider the stochastic process governed by the Fokker–Plack equation

$$\partial_t \begin{pmatrix} \rho_1 \\ \rho_2 \\ \rho_3 \end{pmatrix} = \begin{pmatrix} L(x) - F\partial_x - \gamma & \lambda\gamma & 0 \\ \gamma & L(x) - 2\lambda\gamma & \gamma \\ 0 & \lambda\gamma & L(x) + F\partial_x - \gamma \end{pmatrix} \begin{pmatrix} \rho \\ \rho_2 \\ \rho_3 \end{pmatrix} \tag{32}$$

where $L(x) = \partial_x(v'(x) + KT\partial_x)$. This system is very similar to the fluctuating-force ratchet described in Section 3, only this time a third state is

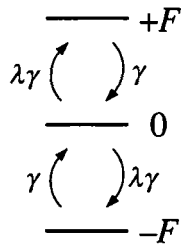

Fig. 7. The stochastic process governing the fluctuating forces used in the three-state ratchet.

included in which the fluctuating force is zero. Figure 7 illustrates the nonequilibrium fluctuations for this process. Note that transitions between states one and three are not allowed and that the parameter λ is a measure of the relative amount of time spent in state 2 as opposed to states 1 and 3. For this process $\phi = 1 + 1/2\lambda$.

The motivation for studying this particular system came from the interesting behavior discovered by Bier that occurs as γ is varied.[21] He found that the current produced by this system changes directions as γ is increased. He then went on to discover that depending on the value of λ he used, not one but two current reversals were possible as γ was increased. These two cases are shown in Figs. 8a and 8b.

Since the second current reversal occurs at high switching rates, i.e., $\gamma \gg 1$, a natural method to use to try and capture this behavior is a small-τ_c perturbation expansion.[19] In this problem there are two types of limiting behavior amenable to perturbative techniques: (1) the fast noise limit and (2) the white noise limit. In the fast noise limit we simply allow γ to become large, holding all other parameters fixed, and use $\tau_c = \gamma^{-1}$ as the smallness parameter in our expansion. In the white noise limit the strength of the fluctuating force is scaled with the correlation time according to

$$F = \left(\frac{D}{\tau_c}\right)^{1/2} \tag{33}$$

with $D = O(1)$ as $\tau_c \to 0$. This type of scaling produces an order-one-weighted delta function correlation function in the nonequilibrium fluctuations as γ becomes large.[8] The details of both perturbation expansions are outlined in the appendix.

In the fast noise limit the current is found to be

$$J = \frac{\tau_c^3}{ZY}\left[\frac{F^4(\phi^2 - 3\phi + 1)}{(\phi KT)^3}\int_0^1 v'(x)^3\,dx - \frac{F^2}{\phi KT}\int_0^1 v'(x)(v''(x))^2\,dx\right] + O(\tau_c^4) \tag{34}$$

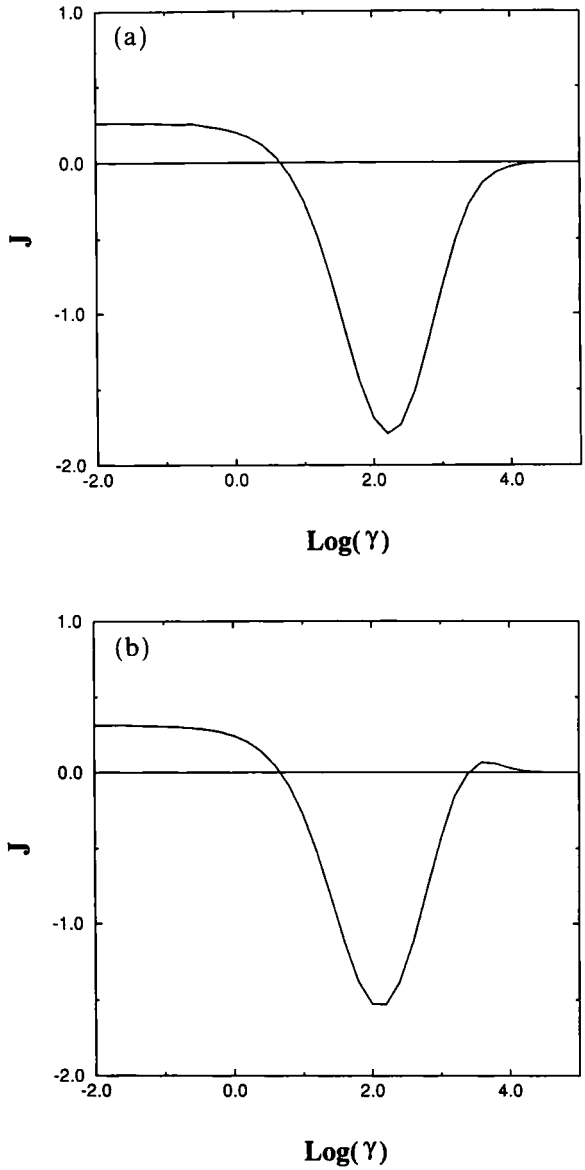

Fig. 8. Plot of the current versus the log of switching rate for the three-state ratchet. The parameters were $E=8$, $F=200.0$, $\alpha=7/8$, and (a) $\lambda=1/3$, (b) $\lambda=1/4$.

where

$$Z = \int_0^1 e^{-v(x)/KT}\, dx \tag{35}$$

and

$$Y = \int_0^1 e^{v(x)/KT}\, dx \tag{36}$$

There are several features of expression (34) worth noting. First of all it predicts a cubic dependence on the smallness parameter τ_c. Second, the sign of the first term in expression (34) depends on the flatness. Because this term goes as F^4 and the second term goes as F^2, we expect for that large enough values of F the first term will dominate and current reversal will occur around $\phi = (3+\sqrt{5})/2 = 2.62$. Note, however, that the integral in the second term contains the square of the second derivative of the potential. For the cases we have considered thus far the potential has been taken to be piecewise linear, and the second derivative of such potentials contains delta functions. The integral of a delta function squared is undefined [formally $\propto \delta(0) = \infty$] and this means that for the piecewise linear potential, the second term in our expansion is infinite! Obviously,

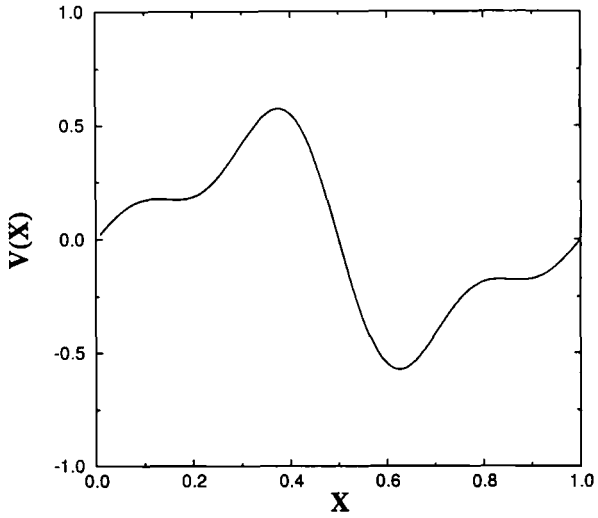

Fig. 9. A plot of one period of the smooth potential given by Eq. (37).

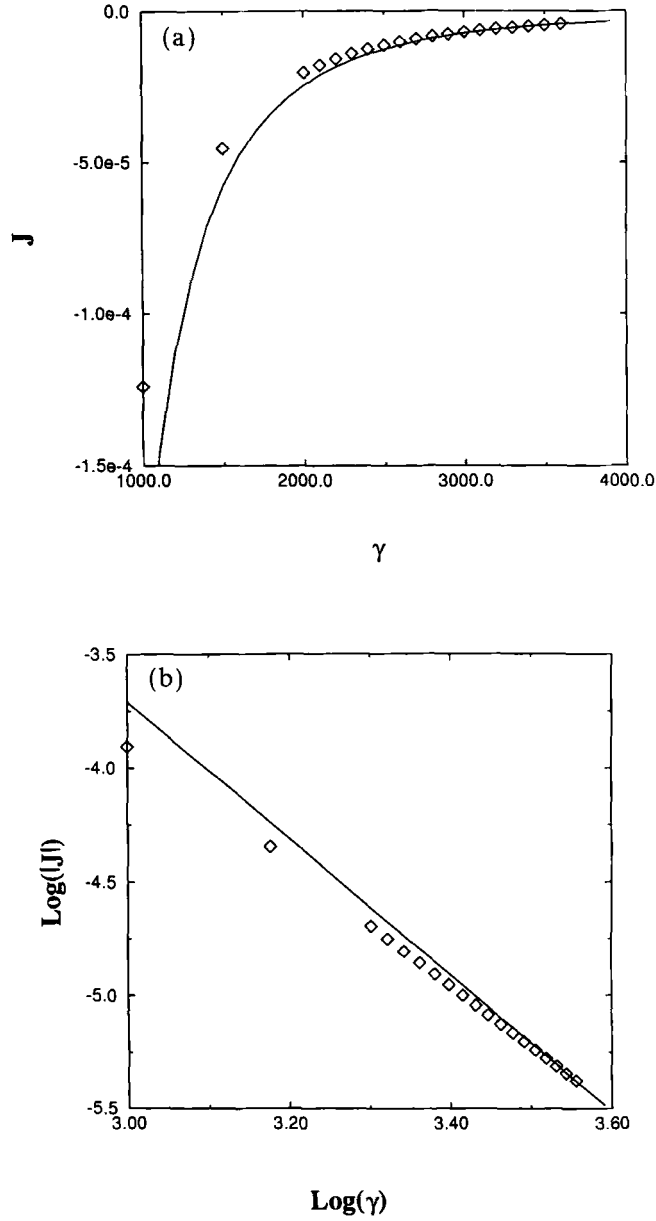

Fig. 10. (a) A plot of the current versus switching rate for the three-state ratchet. The solid line is the fast noise approximation and the diamonds are the numerical results. The parameters used to generate this plot were $KT = 0.3$, $F = 10.0$, $\lambda = 2/5$, and $\Delta x = 1/500$. (b) The same data as in (a), plotted on a log–log plot.

the perturbation expansion we have chosen cannot be valid for nonsmooth potentials. Even for smooth potentials the integral in the second term may be quite large, allowing this term to make considerable contributions to the current.

For the rest of this section we will consider the smooth potential

$$v(x) = \frac{1.25}{\pi}\left(\sin(2\pi x) - \frac{\sin(4\pi x)}{2} + \frac{\sin(6\pi x)}{3}\right) \tag{37}$$

This potential is simply the first three terms of a Fourier series expansion of a piecewise linear potential. One period of this potential is plotted in Fig. 9. Figure 10a is a plot of the current versus switching rate γ. The solid line is the approximation given in (34) and the diamonds are the numerical values obtained using our algorithm. The parameters used to produce this plot were $KT = 0.3$, $F = 10.0$, $\lambda = 2/5$, $\phi = 9/4$, and $\Delta x = 1/500$. Note that the numerics appear to be converging to the asymptotic approximation. Figure 10b is a log–log plot of the same data and clearly shows the convergence.

For the potential given by Eq. (37), the second term in Eq. (34) always produces a positive contribution to the current. If we chose a value of ϕ such that the first term is negative, then Eq. (34) predicts a current reversal as F is decreased. Figure 11 depicts this situation. The same parameters

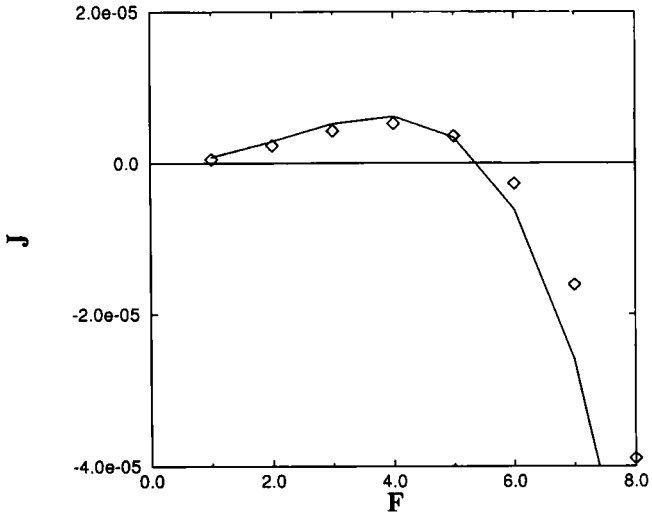

Fig. 11. A plot of the current versus the strength of the fluctuating force F. The same parameters were used to generate this plot as in Fig. 10a, except $\gamma = 1000$.

were used to produce this plot as in Fig. 10, except γ was fixed at 1000 and F was varied. Note that the approximation for the current accurately captures the current reversal and that the approximation is better for smaller values of F, as expected.

In the white noise limit the current is

$$J = \frac{\tau_c D^2}{(\phi\sigma)^3 ZY}(\phi^2 - 3\phi + 1)\int_0^1 v'(x)^3\,dx + O(\tau_c^{3/2}) \tag{38}$$

where $\sigma = (KT + D/\phi)$ and

$$Z = \int_0^1 e^{-v(x)/\sigma}\,dx \tag{39}$$

and

$$Y = \int_0^1 e^{v(x)/\sigma}\,dx \tag{40}$$

Note that the first term in (34) is recovered from (38) in the limit $D = F^2\tau_c \to 0$, but that the second term in (34) involving $(v'')^2$ is lost. Figure 12

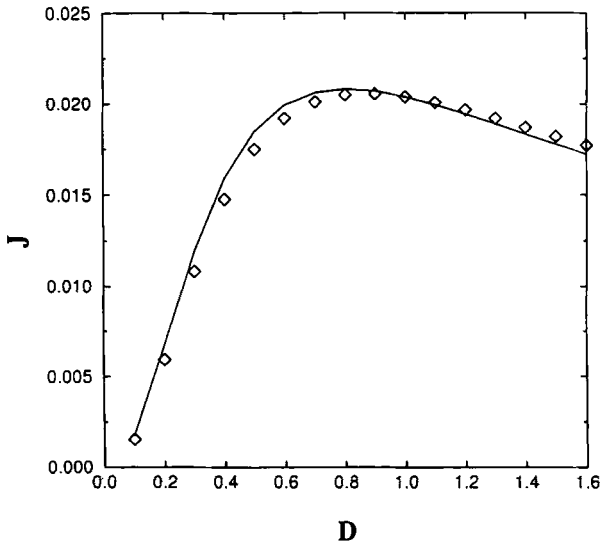

Fig. 12. A plot of the current versus D for the three-state ratchet. The solid line is the white noise approximation and the diamonds are the numerical results. The parameters used to produce this plot were $KT = 0.15$, $\lambda = 1.0$, $\Delta x = 1/350$, and $\gamma = 1000$.

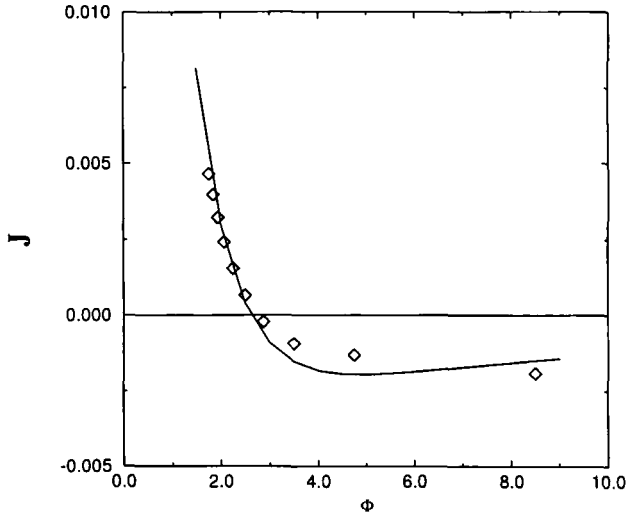

Fig. 13. A plot of the current versus the flatness ϕ. The solid line is the white noise approximation and the diamonds are the numerical results. The parameters used to produce this plot were $KT = 0.15$, $\gamma = 1000.0$, $D = 0.225$, and $\Delta x = 1/350$.

shows a plot of the current versus D. Once again, the solid line is the current computed from Eq. (38) and the diamonds are the numerical results. The parameters used to produce this figure were $KT = 0.15$, $\Delta x = 1/350$, $\lambda = 1$, $\phi = 1$, and $\gamma = 1000$. In the white noise limit the only parameter that determines the direction of the current is the flatness. Equation (38) predicts a flux reversal for a flatness of 2.63. Figure 13 shows a plot of the current versus flatness. The parameters used to produce this plot were $KT = 0.15$, $\gamma = 1000.0$, $D = 0.225$, and $\Delta x = 1/350$. The position of the flux reversal is well captured by the white noise approximation for the current.

5. CONCLUSIONS

We have presented a fast, reliable numerical algorithm for studying noise-induced transport processes. This algorithm has the important feature that it preserves the property of detailed balance for systems in equilibrium. Numerical schemes are frequently designed to preserve important features of the systems they are used to simulate: examples include algorithms that preserve the symplectic structure of Hamiltonian systems and algorithms that conserve the total flux in diffusive systems. A notable difference between those preserved properties and the property of detailed balance is that detailed balance represents a steady-state behavior of the

system and not a specific quantity to be conserved at each time step. The algorithm also provides an efficient means for calculating steady-state probability distributions and currents.

Currently this scheme is only suited for systems whose forces are derivable from gradient vector fields. It is our hope, however, that this method can be generalized to include all force fields. It would also be desirable to extend this algorithm to higher order accuracy. A natural way of doing this might be to allow for the possibility of multiple steps in the jump process. These two issues are the focus of ongoing research.

We have also presented perturbation calculations for a three-state ratchet. The fast noise calculation had the surprising result that it depended on the integral over the square of the second derivative of the periodic potential, which is divergent for piecewise linear potentials. This implies that the expansion we used is not valid for these types of potentials and a rethinking of this calculation is required. We were able to validate the correctness of our calculations for a smooth potential, however.

APPENDIX

We present a brief outline of the perturbation technique used to calculate the asymptotic values of the current presented in Section 4. For convenience the Fokker–Planck equation for the process is written in vector notation

$$\tau_c \partial_t \tilde{\rho} = \tau_c L \mathbf{I} \tilde{\rho} - \tau_c F \partial_x \mathbf{J} \tilde{\rho} + \mathbf{K} \tilde{\rho} \tag{A1}$$

where $\tilde{\rho} = (\rho_1, \rho_2, \rho_3)$, the matrices $\mathbf{K}$ and $\mathbf{J}$ are defined to be

$$\mathbf{K} = \begin{pmatrix} -1 & \lambda & 0 \\ 1 & -2\lambda & 1 \\ 0 & \lambda & -1 \end{pmatrix}, \qquad \mathbf{J} = \begin{pmatrix} 1 & 0 & 0 \\ 0 & 0 & 0 \\ 0 & 0 & -1 \end{pmatrix} \tag{A2}$$

and $\mathbf{I}$ is the identity matrix. The first step in the calculation is to determine the right eigenvectors and eigenvalues of the matrix $\mathbf{K}$. The eigenvectors are

$$\tilde{Q}_0 = \begin{pmatrix} \lambda/(1+2\lambda) \\ 1/(1+2\lambda) \\ \lambda/(1+2\lambda) \end{pmatrix}, \qquad \tilde{Q}_1 = \begin{pmatrix} \lambda/(1+2\lambda) \\ 0 \\ -\lambda/(1+2\lambda) \end{pmatrix}, \qquad \tilde{Q}_2 = \begin{pmatrix} \lambda/(1+2\lambda) \\ -2\lambda/(1+2\lambda) \\ \lambda/(1+2\lambda) \end{pmatrix} \tag{A3}$$

and have eigenvalues 0, -1, and $-(1+2\lambda)$, respectively. In the fast noise limit, the stationary solution of Eq. (A1) is constructed in terms of integer powers of τ_c, i.e.,

$$\tilde{\rho}_s = \tilde{\rho}_s^{(0)} + \tau_c \tilde{\rho}_s^{(1)} + \tau_c^2 \tilde{\rho}_s^{(2)} + \cdots \tag{A4}$$

The current may be expressed as

$$J = j^{(0)} + \tau_c j^{(1)} + \tau_c^2 j^{(2)} + \cdots \tag{A5}$$

where the τ_c^n contribution to the steady-state current is

$$j^{(n)} = \tilde{Q}_0^{\dagger}[\, -(v'(x) + KT\partial_x)\, \mathbf{I} + F\mathbf{J}\,]\, \tilde{\rho}^{(n)} \tag{A6}$$

with $\tilde{Q}_0^{\dagger} = (1, 1, 1)$ the left eigenvector of the matrix $\mathbf{K}$ with eigenvalue zero. The terms in the expansion for $\tilde{\rho}_s$ satisfy the equations

$$0 = \mathbf{K}\tilde{\rho}_s^{(0)} \tag{A7}$$

$$0 = \mathbf{K}\tilde{\rho}_s^{(1)} + (L\mathbf{I} + F\partial_x \mathbf{J})\, \tilde{\rho}_s^{(0)} \tag{A8}$$

$$0 = \mathbf{K}\tilde{\rho}_s^{(2)} + (L\mathbf{I} + F\partial_x \mathbf{J})\, \tilde{\rho}_s^{(1)} \tag{A9}$$

$$0 = \mathbf{K}\tilde{\rho}_s^{(3)} + (L\mathbf{I} + F\partial_x \mathbf{J})\, \tilde{\rho}_s^{(2)} \tag{A10}$$

The eigenvectors of $\mathbf{K}$ form a convenient basis in which to expand solutions of these equations. We must therefore determine the action of the matrix $\mathbf{J}$ on the Q vectors. We find

$$\mathbf{J}\tilde{Q}_0 = \tilde{Q}_1 \tag{A11}$$

$$\mathbf{J}\tilde{Q}_1 = \frac{2\lambda}{1+2\lambda}\, \tilde{Q}_0 + \frac{1}{1+2\lambda}\, \tilde{Q}_2 \tag{A12}$$

$$\mathbf{J}\tilde{Q}_2 = \tilde{Q}_1 \tag{A13}$$

We now successively solve Eqs. (A7)–(A10). The solution of Eq. (A7) is

$$\tilde{\rho}_s^{(0)} = r_0(x)\, \tilde{Q}_0 \tag{A14}$$

where $r_0(x)$ is an undetermined function of x. The functional form of r_0 will be determined when the equation for $\tilde{\rho}^{(1)}$ is solved. This will continue to be the case as we solve for the higher order terms in the expansion. That is, the nth-order equation will only determine $\tilde{\rho}^{(n)}$ up to an unknown term of

the form $r_n(x)\,\tilde{Q}_0$. However, for $n>0$ this is sufficient to calculate the nth-order contribution to the current. Up to third order in τ_c we find

$$\tilde{p}^{(1)} = r_1(x)\,\tilde{Q}_0 - F\partial_x r_0(x)\,\tilde{Q}_1 \tag{A15}$$

$$\tilde{p}^{(2)} = r_2(x)\,\tilde{Q}_0 - F(L\partial_x r_0 + \partial_x r_1)\,\tilde{Q}_1 + \frac{F^2}{(1+2\lambda)^2}\partial_x^2 r_0 \tilde{Q}_2 \tag{A16}$$

$$\tilde{p}^{(3)} = r_3(x)\,\tilde{Q}_0 - F\left(L(L\partial_x r_0 + \partial_x r_1) + \partial_x r_2 + \frac{F^2}{(1+2\lambda)^2}\partial_x^3 r_0\right)\tilde{Q}_1 + \frac{F^2}{(1+2\lambda)^2}\left(\frac{1}{1+2\lambda}L\partial_x^2 r_0 + \partial_x(L\partial_x r_0 + \partial_x r_1)\right)\tilde{Q}_2 \tag{A17}$$

where

$$r_0(x) = \frac{e^{-v(x)/KT}}{Z} \tag{A18}$$

$$r_1(x) = \frac{2\lambda F^2 r_0}{(KT)^2(1+2\lambda)}\left[v(x) - \langle v(x)\rangle\right] \tag{A19}$$

$$r_2(x) = \frac{2F^2\lambda r_0}{KT(1+2\lambda)}\left\{v''\frac{(v')^2}{2KT} - \frac{\langle (v')^2\rangle}{KT} + \frac{2\lambda F^2}{(KT)^2(1+2\lambda)}(\langle v\rangle - v) + \frac{2\lambda F^2}{(KT)^3(1+2\lambda)}\left[\frac{1}{2}(v^2 - \langle v^2\rangle) - v\langle v\rangle + \langle v^2\rangle\right]\right\} \tag{A20}$$

The brackets in Eqs. (A19) and (A20) indicate averaging over one period of the potential $v(x)$ with respect to $r_0(x)$. Equation (A6) can now be used to calculate the current up to third order in τ_c. When this is done, the first nonzero contribution to the current turns out to be $j^{(3)}$ and is exactly expression (34) of Section 4.

In the white noise limit the strength of the fluctuating force F is scaled with τ_c in the following way: $F=(D/\tau_c)^{1/2}$. This scaling is used so that in the limit of small τ_c, the correlation function of the fluctuating-force process approaches a delta function. The perturbation calculation for the white noise limit is identical to the fast noise limit, only this time the expansion of $\tilde{p}$ is in powers of $\tau_c^{1/2}$, i.e.,

$$\tilde{p}_s = \tilde{p}_s^{(0)} + \tau_c^{1/2}\tilde{p}_s^{(1/2)} + \tau_c^{1}\tilde{p}_s^{(1)} + \cdots \tag{A21}$$

and the $j^{(n/2)}$ contribution to the current is given by

$$j^{(n/2)} = \tilde{Q}^{\dagger}\left[-(v'(x) + KT\partial_x)\,\mathbf{I}\tilde{p}^{(n/2)} - D^{1/2}\partial_x \mathbf{J}\tilde{p}^{(n/2+1/2)}\right] \tag{A22}$$

The terms in the expansion (A21) of $\tilde{\rho}_S$ now satisfy the equations

$$0 = \mathbf{K}\tilde{\rho}^{(0)} \tag{A23}$$

$$0 = \mathbf{K}\tilde{\rho}^{(1/2)} + D^{1/2}\partial_x \mathbf{J}\tilde{\rho}^{(0)} \tag{A24}$$

$$0 = \mathbf{k}\tilde{\rho}^{(1)} + D^{1/2}\partial_x \mathbf{J}\tilde{\rho}^{(1/2)} + L\mathbf{I}\tilde{\rho}^{(0)} \tag{A25}$$

and the procedure continues exactly as before. This time the first nonzero contribution to the current is the $j^{(1)}$ term and is given as Eq. (38) in Section 4.

ACKNOWLEDGMENTS

The authors would like to thank Martin Bier and George Oster for stimulating conversations. We also thank Martin Bier for providing the data for the curves shown in Figs. 5 and 8. This work was supported by the DOE and NSF.

REFERENCES

1. M. Magnasco, *Phys. Rev. Lett.* **71**:1477 (1993).
2. J. Maddox, *Nature* **365**:203 (1993).
3. M. Millonas and M. Dykman, *Phys. Lett. A* **185**:65 (1994).
4. C. Peskin, G. Ermentrout, and G. Oster, *Cell Mechanics and Cellular Engineering* (Springer-Verlag, Berlin, 1994).
5. R. Astumian and M. Bier, *Phys. Rev. Lett.* **72**:1766 (1994).
6. J. Maddox, *Nature* **368**:287 (1994).
7. J. Prost, J. Chauwin, L. Peliti, and A. Adjari, *Phys. Rev. Lett.* **72**:2652 (1994).
8. C. Doering, W. Horsthemke, and J. Riordan, *Phys. Rev. Lett.* **72**:2984 (1994).
9. J. Maddox, *Nature* **369**:181 (1994).
10. J. Rousselet, L. Salome, A. Adjari, and J. Prost, *Nature* **370**:446 (1994).
11. S. Leibler, *Nature* **369**:412 (1994).
12. R. Bartussek, P. Hanggi, and J. G. Kissner, *Europhys. Lett.* **28**:459 (1994).
13. K. Svoboda and S. Block, *Cell* **77**:773 (1994).
14. K. Svoboda, P. Mitra, and S. Block, *Proc. Natl. Acad. Sci. USA* **91**:11782 (1994).
15. C. Peskin and G. Oster, *Biophys. J.* **68**:202s (1995).
16. C. Gardiner, *Handbook of Stochastic Processes* (Springer-Verlag, Berlin, 1983).
17. W. Press, B. Flannery, S. Teukolsky, and W. Vetterling, *Numerical Recipes* (Cambridge University Press, Cambridge, 1988).
18. C. Doering, In Proceedings of the Workshop on Fluctuations in Physics and Biology, *Nuovo Cimento* **17**:685 (1995).
19. W. Horsthemke and R. Lefever, *Noise Induced Transitions* (Springer, New York, 1984).
20. N. Van Kampen, *Stochastic Processes in Physics and Chemistry* (North-Holland, Amsterdam, 1981).
21. M. Bier, *Phys. Lett. A* **211**:12 (1996).